A PZT-PVDF Stacked Transducer for Short-pulse Ultrasound Therapy and Monitoring

Zheng Jiang, Robert J. Dickinson, Timothy L. Hall, and James J. Choi

Abstract—Therapeutic ultrasound technologies using microbubbles require a feedback control system to perform the treatment in a safe and effective manner. Current feedback control technologies utilize the microbubble's acoustic emissions to adjust the treatment acoustic parameters. Typical systems use two separated transducers: one for transmission and the other for reception. However, separating the transmitter and receiver leads to foci misalignment. This limitation could be resolved by arranging the transmitter and receiver in a stacked configuration. Taking advantage of an increasing number of short-pulse-based therapeutic methods, we have constructed a PZT-PVDF stacked transducer design that allows the transmission and reception of short-pulse ultrasound from the same location. Our design had a piston transmitter composed of a PZT disc (1 MHz, 12.7 mm in diameter), a backing layer, and two matching layers. A layer of Polyvinylidene fluoride (PVDF) (28 µm in thickness, 12.7 mm in diameter) was placed at the front surface of the transmitter for reception. Transmission and reception from the same location was demonstrated in pulse-echo experiments where PZT transmitted a pulse and both PZT and PVDF received the echo. The echo signal received by the PVDF was 0.43 µs shorter than the signal received by the PZT. Reception of broadband acoustic emissions using the PVDF was also demonstrated in experiments where microbubbles were exposed to ultrasound pulses. Thus, we have shown that our PZT-PVDF stack design has unique transmission and reception features that could be incorporated into a multi-element array design that improves focal superimposing, transmission efficiency, and reception sensitivity.

Index Terms—Short-pulse ultrasound, stacked transducer, therapy and monitoring.

I. INTRODUCTION

The expansion and contraction of microbubbles in an acoustic field is under investigation for use in therapeutic ultrasound systems to treat diseases. Microbubbles are micron-sized bubbles that typically have a stable gas core encased in a lipid or polymer shell. When the injected microbubbles are exposed to an acoustic field, they not only reflect the sound, but also generate their own unique acoustic emissions, such as sub-harmonics (f_0/m, where f_0 is the fundamental frequency and m is an integer value), harmonics, ultra-harmonics (nf_0/m, where n is also an integer value), and broadband signals. To improve the performance and safety of the therapeutic procedure, feedback control technologies based on detecting microbubble emissions have been developed [1-5]. The detection of subharmonics [6], harmonics [1] or ultra-harmonics [7] from microbubbles has been used to adjust the sonication pressure to produce safer and more effective treatments. Broadband emissions suggest tissue damage [8], and primarily arise from the inertial collapse of a microbubble. Such collapses apply strong mechanical forces on the tissue microenvironment, hence they should be carefully monitored as well. Such feedback technologies require the generation and reception of ultrasound at different frequencies. In principle, it is possible to construct very high bandwidth single-element transducers that transmit at fundamental frequency and receive microbubble emissions in a broad frequency range, but this would have a large trade-off between transmission efficiency and reception bandwidth. Hence, the generation and reception of ultrasound are typically achieved by using different transducers.

There are two broad categories of dual-frequency transducers, namely interleaved and stacked designs [9]. In interleaved designs, which are the most commonly used arrangement, the structure is typically a focused single-element transmitter with a receiver in the center [10] or a multi-element transmitter array with receivers distributed on the same hemispherical surface [11, 12]. The transmitters are lead zirconate titanate (PZT), while the receivers are PZT [13] or Polyvinylidene fluoride (PVDF). Although straightforward to build and repair, such interleaved transducers have natural shortcomings. For those using a single focused transmitter and a receiver, aligning their foci is challenging. As for an interleaved multi-element array, the transmitters are densely distributed which leaves very limited space for receivers. This not only introduces a trade-off between transmission efficiency and reception sensitivity, but also increases the design and fabrication complication. Some practical improvements have been made to interleaved multi-element array designs. For example, cylindrical transmitters are used in some designs [11, 14] so that the receivers can fit within the hollow centre of transmitters [15]. These designs are easy to fabricate but the transmission efficiency is still sacrificed.

Stacked designs where the receiver is mounted on top of the transmitter could improve receiving sensitivity without large compromises to the transmitting performance, but two concerns have limited their use in microbubble-mediated therapeutic applications. First, the transmitted therapeutic pulse and the received microbubble emissions superimposing at the

UK. (e-mail: zheng.jiang18@imperial.ac.uk; robert.dickinson@imperial.ac.uk; j.choi@imperial.ac.uk).

Timothy L. Hall is with the Department of Biomedical Engineering, University of Michigan, Ann Arbor, MI 48109, USA. (e-mail: hallt@umich.edu).

receiver's surface. In ultrasound-mediated drug delivery (e.g., blood-brain barrier (BBB) opening), long sonication pulses are typically 2 to 10 ms in duration [7, 12], so the received signals from superficial microbubbles will coincide with the transmitted pulses. Second, stacked configurations restrict the designer's ability to select the best backing and matching layers for both the transmitter and receiver. In most stacked designs, two layers of PZT are used with the one for transmitting placed beneath the one for receiving. Hence, a matching layer in between [16] must be carefully designed to reduce the ringing of received signals and crosstalk between the two PZT layers. Furthermore, the PZT receiver is limited to a relatively narrow frequency range, which leads to a limited ability in receiving broadband signals. A potentially better approach is to use a PZT-PVDF stacked design, allowing efficient transmission with the PZT and broadband reception with the PVDF. Initial designs were for ultrasound imaging, to improve the image quality by either placing the PVDF on top of existing ultrasound imaging probes [17, 18] or designing new PZT-PVDF stacks [19, 20]. However, there have been no PZT-PVDF stack designed and tested for therapeutic use or with microbubbles within the clinically relevant size range of 1 to 10 µm in diameter.

In recent years, an increasing number of short-pulse therapeutic ultrasound methods have been developed. Histotripsy, which is a method of using ultrasound to produce mechanical disruption of tissue, uses short-pulse ultrasound (< 20µs) [21, 22]. Short pulses on the order of microseconds have also been shown to improve the uniformity of drug delivery across the BBB [23, 24], decrease treatment time [25], and potentially reduce risk of causing damage [26]. We have previously shown that short ultrasound pulses (5 µs in duration) with injected microbubbles can safely and effectively open the BBB [27]. By using short pulses, the superimposing of transmitted and received signals can be avoided.

We designed a new PZT-PVDF stack that could be used for short-pulse therapeutic ultrasound applications. In this design, PVDF is used for its good receiving sensitivity [28] and its broadband frequency response, even without a backing layer. Since the acoustic impedance of PVDF is similar to water, a matching layer was not required when directly interfaced with water. As the thickness of a PVDF sheet is normally on the order of micrometers, we did not expect it to significantly affect the transmission performance of PZT. Hence, the stacked transducer was simplified as a traditional piston transducer design, where the backing and matching layers were selected solely for the PZT. In the following sections, we first introduce the structure of our stacked transducer and the pre-amplifier for the PVDF receiver. We then evaluate the stacked transducer's ability to transmit and receive ultrasound from the same location in a pulse-echo experiment. Finally, we evaluate the PVDF's ability to receive signals in a broad frequency range by detecting acoustic emissions from microbubbles exposed to ultrasound. The receiving performance of PVDF was compared to PZT.

II. MATERIALS AND METHODS

A. PZT-PVDF stacked transducer design and construction

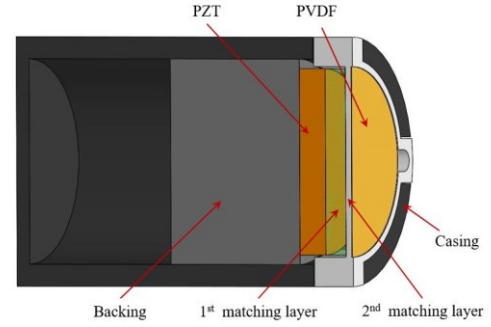The stacked transducer was composed of a PZT transmitter

Fig. 1. A cross-sectional image of the PZT- PVDF stacked transducer.

with a PVDF receiver mounted on its front. From back to front, the stacked transducer consisted of a backing layer, a PZT disc (1 MHz, Navy type II/Pz27, Meggitt A/S, Denmark), the 1st matching layer, the 2nd matching layer, and a PVDF sheet that had metallized electrodes and poling across the entire surface (28 µm-in-thickness, Precision Acoustics, UK). Both the PZT and PVDF are 12.7 mm in diameter. These components were enclosed in a 3D-printed casing (Fig. 1).

The PZT transmitter was designed to transmit short pulses hence a heavy backing and two matching layers were used. The backing layer was a mixture of tungsten powder (12 µm, Sigma-Aldrich, UK) and epoxy (3421, Loctite, Germany) with a mixing ratio of 80/20 (w/w, its impedance is about 6 MRayl) [29]. The 1st matching layer was a 1.57-mm-thick glass disc and the 2nd matching layer was a 0.45-mm-thick 3D printed disc (Veroclear, Objet 30 Pro, Stratasys Ltd. Israel). The two matching layers were both selected with a thickness close to one-quarter wavelength. Their acoustic impedance was determined as the following [30],

$$Z_{m1} = \left(Z_p{}^4 Z_l{}^3\right)^{1/7}$$
$$Z_{m2} = \left(Z_p Z_l{}^6\right)^{1/7}$$

where Z_{m1}, Z_{m2}, Z_p, and Z_l are the acoustic impedance of the 1st matching layer, the 2nd matching layer, PZT, and water, respectively (Table I). The 2nd matching layer was also designed to hold the PZT, PVDF, and the 1st matching layer as a sub-assembly unit.

The stack of components (PZT, PVDF, and two matching layers) was first mounted together using epoxy (Araldite standard, Antala Ltd, UK). Then, it was assembled onto a 3D printed casing (PLA, Ultimaker 2+, Ultimaker, Netherlands), localized by the guide pins and fixed with epoxy (Araldite standard, Antala Ltd, UK). The backing layer was filled into the casing after. The casing was then sealed, ensuring a waterproof stacked transducer.

TABLE I
PROPERTIES OF THE MATERIALS IN THE STACKED TRANSDUCER AND THE IDEAL MATCHING LAYERS

Material	Impedance (MRayl)	Sound speed (m/s)	Thickness (mm)
Pz27	34	/	2
PVDF	4	/	0.028
Glass (1st matching)	13	6000	1.57
Veroclear (2nd matching)	2.1	1791	0.45
Z_{m1}	8.9	/	1.5
Z_{m2}	2.3	/	0.45

B. Pre-amplifier design and characterization

A JFET operational amplifier OPA659 (Texas Instruments, USA) was selected to build a pre-amplifier for the PVDF receiver (Fig. 2a). As OPA659 has a large bandwidth (650-MHz unity-gain), the pre-amplifier will not overly limit the bandwidth of the PVDF receiver. The frequency response of the pre-amplifier was evaluated by adjusting the frequency of a sinusoidal input from a function generator (33500B series,
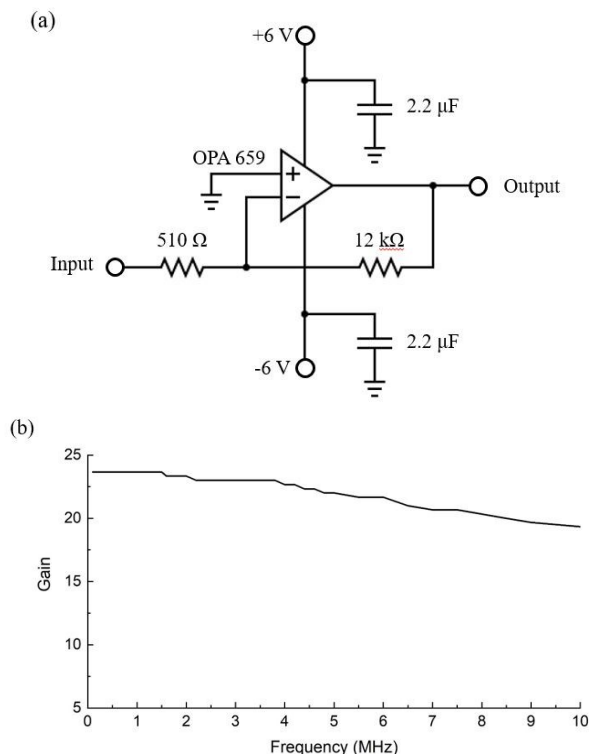

Fig. 2. The pre-amplifier designed for the PVDF receiver. (a) Circuit diagram. (b) Frequency response of the pre-amplifier.

Agilent Technologies, Inc., USA) while recording the output with an oscilloscope (Tektronix DPO3014, Tektronix, Inc., USA). The pre-amplifier provided a reasonably good gain over a wide frequency range. The gain remained stable at 23.5 until 1.5 MHz, where it then dropped slowly to 19 at 10 MHz (Fig. 2b).

C. Pulse-echo performance

The stacked transducer's ability to transmit and receive ultrasound simultaneously from the same location was evaluated in pulse-echo mode against a near-perfect reflector (Fig. 3a). The PZT was excited by a pulser/receiver system (DPR 300, JSR Ultrasonics, USA). The transmitted ultrasound pulses traveled 15 cm, reflected from a thick metal plate, and captured by the PZT and PVDF. The PZT and PVDF signals were then amplified by the pulser/receiver's internal amplifier (Gain: 25) and our custom pre-amplifier (Fig. 2a), respectively, and recorded using an oscilloscope (Tektronix DPO3014, Tektronix, Inc., USA).

The quality of the PZT and PVDF reception signals was compared to the same pulse captured with a 1 mm-in-diameter needle hydrophone (Precision Acoustics, UK) (Fig. 3b). A pulse was transmitted with the same PZT and pulser/receiver, but captured with a hydrophone placed 30 cm away from the front surface of the stacked transducer.

Since there were two matching layers (a 1.57-mm-thick glass and a 0.45-mm-thick Veroclear material) between the PZT and PVDF, there was a slight difference on time of arrival. We adjusted the time of arrival according to the calculated delay to align the two signals for better comparison. Both signals were then compared to the hydrophone signal.

D. Microbubble emission detection

1. Experimental setup

The stacked transducer's ability to detect microbubbles' acoustic emissions was evaluated using a channel of microbubbles exposed to ultrasound (Fig. 4). The experiment was performed in a tank filled with deionised and degassed water. The stacked transducer was intended to be one element of a multi-element array so this single module was not expected to generate a high enough acoustic pressure on its own to get therapeutically-relevant microbubble acoustic emissions. As a result, we used a separate focused 1 MHz transducer (Olympus, Japan) to sonicate the microbubbles. Its focal length was 75 mm and its axial full width at half maximum (FWHM) and lateral FWHM were 55 mm and 3 mm, respectively. Saline and microbubble solution or saline alone (control) flowed through a
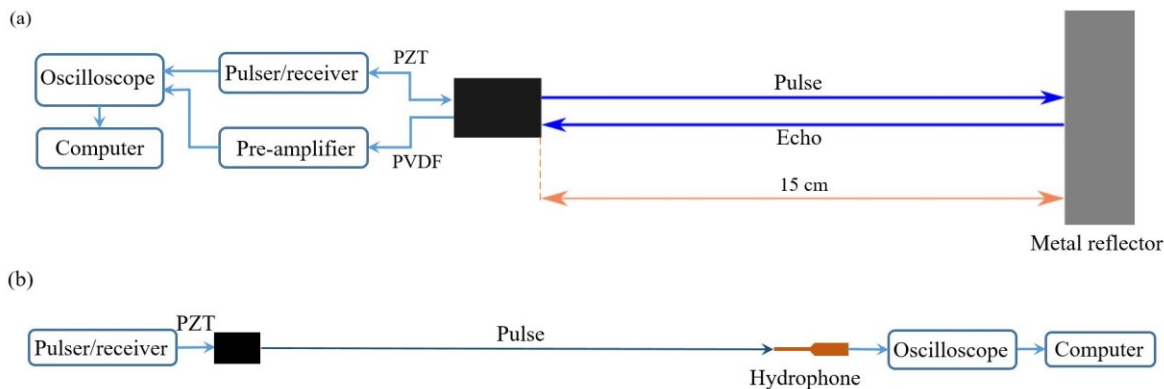

Fig. 3. Pulse-echo experimental setup. (a) The experimental setup used to evaluate the stacked transducer's pulse-echo performance. The stacked transducer faced a metal reflector and its 1-MHz PZT transmitter was excited by a pulser/receiver. The reflected echo was captured by both the PZT and PVDF. The signals were then amplified before being visualized on an oscilloscope and stored on a computer. (b) The experimental setup used to capture the gold standard pulse signal transmitted by the same PZT. The PZT was excited by the pulse/receiver and the signal was captured by a needle hydrophone with a 1-mm diameter located 30 cm away.

0.63 mm-in-diameter wall-less channel within a block of hydrogel, which overlapped with the focal spot of the focused transducer and was perpendicular to the direction of ultrasound wave propagation. The stacked transducer was used to receive the microbubbles' acoustic emissions. It was aligned facing the sonicated channel region at a distance of 95 mm and with an angle of 20 degrees clockwise from the direction of wave propagation.

The wall-less channel was made of polyacrylamide hydrogel and had a modulus of elasticity of 8.44 ± 0.82 kPa [31]. The relatively soft gel was selected to minimise the effects of rigid confinement and acoustic reflections from the gel-water interface. It was cast in a 3D printed mould with a 0.63 mm-in-diameter nylon wire. The wire was removed after the hydrogel cured to form a 0.63 mm-in-diameter channel. The diameter was selected to allow enough microbubbles to be present within the volume to generate sufficient acoustic emissions.Cellulose tubes were inserted into both ends of the channel for the syringe to draw liquid through.
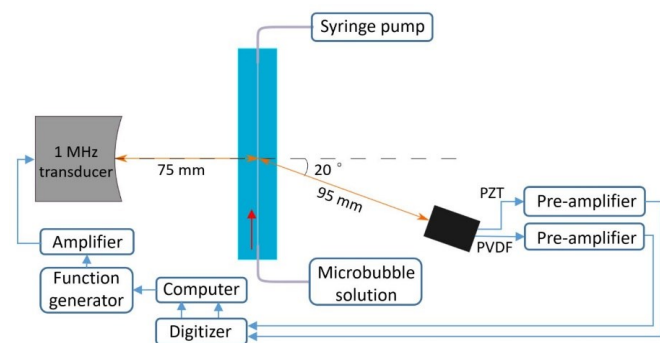

Fig. 4. Experimental setup for microbubble emission detection. Microbubbles flowing inside a 0.63 mm-in-diameter channel were sonicated by a 1 MHz focused transducer. The PZT and PVDF stacked transducer was aligned facing the sonicated channel region. The signals captured by PZT and PVDF were amplified and digitized before recorded by a computer.

In-house manufactured microbubbles [32, 33] were used in the experiment. Dipalmitoylphosphatidylcholine (DPPC-82%), dipalmitoylphosphatidic acid (DPPA-8%), and dipalmitolyphosphatidylethanolamine–PEG5000 (DPPE–PEG5000-10%) were first mixed and diluted with saline and glycerol. Perfluorobutane was then added and the mixture was amalgamated. The microbubble suspension was diluted with saline at a ratio of 1: 1000. The microbubble solution was constantly stirred by a magnetic stirrer, and was drawn through the channel by a syringe pump (Harvard Apparatus, US). The pulling speed was 0.2 ml/min which generated an estimated fluid velocity of 11.4 mm/s inside the channel.

The 1 MHz Olympus transducer was excited by a function generator (33500B series, Agilent Technologies, Inc., USA) through a power amplifier (2100L, Electronics & Innovation Ltd, USA). The microbubbles' acoustic emissions were captured with the PVDF and PZT, and subsequently amplified by our designed pre-amplifier (Fig. 2) and a 25x amplifier (SIM914, Stanford Research Systems, USA), respectively. The amplified signals were then digitized by GaGe digitizer (Oscar 16, Dynamic Signals, USA) and recorded by a computer.

2. Sonication and data processing

As we were only interested in the microbubble's acoustic emissions signal, the primary sonication pulse's reflections and reverberations were removed. A control group with 10 trials was first recorded, where only saline solution was administered into the channel. A microbubble group was then run where the diluted microbubbles were exposed to ultrasound. In both groups, acoustic signals were captured with the PZT and PVDF transducers. In each set of experiments, pulses (centre frequency: 1 MHz, pulse length: 5 cycles) were transmitted with a range of peak-negative pressure (PNP): 0.4 MPa to 1.3 MPa with an increasing step of 0.1 MPa. Ten trials were run for the control group and for each pressure. We selected a 2-second gap between pulses, so that microbubbles could replenish the focal volume. Since the microbubbles flowed at a 11.4 mm/s fluid velocity, the 2 seconds allowed the microbubbles to travel 22.8 mm between pulses, far longer than the width of the ultrasound beam and its side lobes.

The background signal was obtained by averaging the 10 control trials in the time domain. The microbubble emission signals were then obtained by subtracting the background signal from each microbubble trial signal in the time domain [34]. The background-subtracted signals were then analyzed and compared in the time and frequency domains.

III. RESULTS

A. Pulse-echo performance

The stacked transducer was able to transmit pulses with the PZT (Fig. 5a) and receive the reflected echo with both the PZT and the PVDF (Fig. 5b). This demonstrated that our stacked transducer could transmit and receive short pluses from the same location.

The needle hydrophone signal (Fig. 5a) was used as the gold standard reference. The duration defined as the full width at half
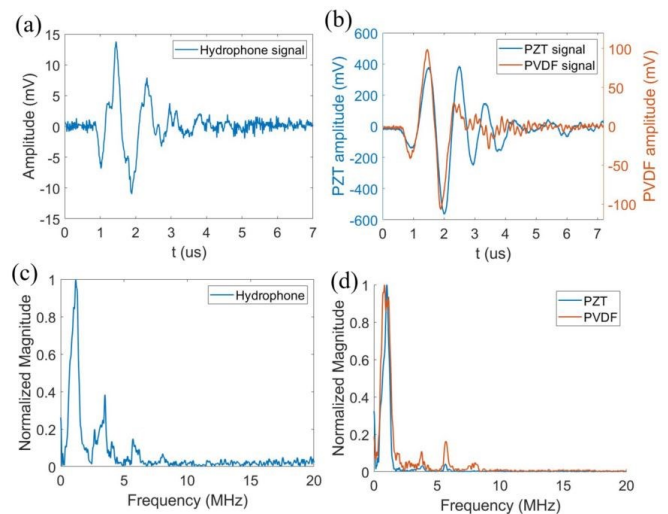

Fig. 5. Pulse-echo with the PZT and PVDF stack. (a) A pulse was generated by the PZT using a pulser/receiver. The signal was captured by a 1-mm-in-diameter needle hydrophone placed 30 cm away from the stacked transducer. A metal reflector then replaced the location of the needle hydrophone. (b) Echo signals from the metal reflector were received by the PZT and PVDF of the stacked transducer. The frequency domain of the signals received with the (c) hydrophone and (d) PZT and PVDF were calculated.

maximum (FWHM) of the signal envelope from the hydrophone was 1.30 μs. Lower amplitude high frequency 'spikes' were also observed. The higher frequency signals were due to the PZT being excited by an impulse, driving the PZT not only at its resonant frequency, but also at its odd-integer harmonics (Fig. 5c).

As there were two matching layers between the PZT and PVDF, the echo signal arrived at different times. For better qualitative comparison, the PVDF signal was manually delayed by 0.75 μs to align with the PZT signal (Fig. 5b). The PVDF signal was shorter than the PZT signal. Whereas the signal captured by the PVDF had a duration of 1.12 μs, the signal captured by the PZT had a duration of 1.55 μs due to ringing. The amplitude of the PZT signal was approximately 5 times larger than the PVDF signal. There were a lot more higher frequency components in the echo received by the PVDF. With respect to duration, pulse shape, and frequency components, the received echo signal with the PVDF resembled the hydrophone signal more closely than with the PZT (Fig. 5). We also measured the -6 dB bandwidth of the PZT to be 60 %.

B. Microbubble emission detection

Acoustic emissions from the microbubbles were detected by both the PZT and PVDF (Fig. 6). However, the signals detected by them were different in both time and frequency domains.

In the time domain, the signal captured by the PZT (Fig. 6a) had a higher contribution from a single frequency than the signal captured by the PVDF (Fig. 6c). This is because the signals captured by PZT were mainly around 1 MHz, where it was the most sensitive. Unlike PZT, PVDF was able to capture signals with a much broader bandwidth, hence the waveform had sharper features. The duration of the main pulse from PZT was longer than that from PVDF. This was caused by the lower bandwidth of the PZT.

In the frequency domain, the signal received from the PZT was mainly at 1 MHz with very weak components at 3-4 MHz,
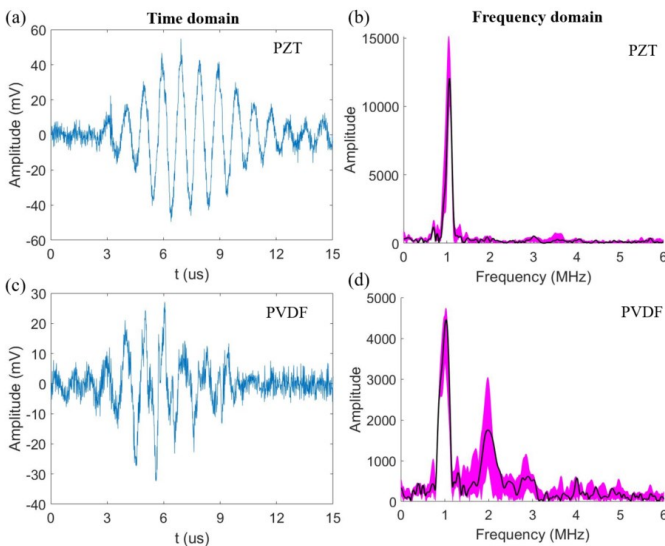
Fig. 6. Microbubble emissions received by the PZT and PVDF. Time traces of the detected microbubble emissions from (a) PZT and (c) PVDF, and their Fourier magnitude spectrum (b) and (d), respectively. The shaded areas in (b) and (d) are the range of 10 trials, and the line was one data set of them. The sonication pulse parameters were 1 MHz, 5 cycles, and 0.4 MPa.

which was the 3rd harmonic frequency of the PZT (Fig. 6b). On the other hand, the signal received from PVDF (Fig. 6d) had large contributions from sub-harmonics, higher order harmonics, and ultra-harmonics, which were expected from microbubble acoustic emissions under a 5-cycle sonication pulse.

PVDF was compared to PZT for a range of peak-negative pressures (0.4 to 1.3 MPa) (Fig. 7). PZT mainly received signals at its odd-order harmonic frequencies at all pressures evaluated (Fig. 7a). Meanwhile, PVDF had a far broader frequency sensitivity (Fig. 7b). At low pressures, the signals captured by PVDF were mainly at harmonic frequencies. As sonication pressure increased to 0.6 MPa, more broadband signals were observed, which might be caused by microbubble collapse (Fig. 7b). As broadband microbubble emissions are normally the indicator of tissue damage [8], PZT's poor ability to capture broadband signals limit its ability to provide feedback to a control unit, especially when the therapeutic pulse is short in length.
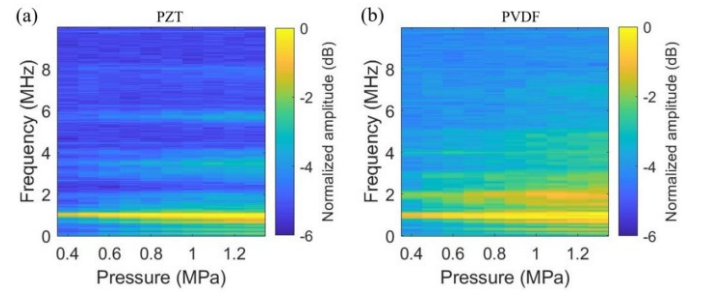
Fig. 7. Normalized frequency spectrum of microbubble emissions captured by (a) PZT and (b) PVDF. The data was averaged across 10 trials in frequency domain.

IV. DISCUSSION

We demonstrated that a PZT-PVDF stacked transducer can be used in pulse-echo mode, transmitting short pulses with the PZT and receiving from both the PZT and PVDF. The stacked transducer can also be used to monitor acoustic emissions generated from microbubbles. This stacked transducer works with short pulses and can be easily incorporated into multi-element arrays.

The PVDF captured signal (Fig. 5b and 5d) was close to the ground truth signal obtained with a needle hydrophone both in the time and frequency domains (Fig. 5a and 5c), outperforming the PZT. The tail after the main pulse received by the PVDF was different from the hydrophone signal, which could be caused by rough surfaces of the reflector, the crosstalk from PZT, and surface averaging caused by the PVDF receiver's large active area. Although the pulse-echo performance of the PZT in our stacked transducer was fairly good (a -6 dB bandwidth of 60 %), producing similar result to other studies [35-37], the echo signal that the PZT received had ringing artifacts, which lengthened the received pulse. This demonstrates an advantage of using PVDF as the receiver over PZT. Note that our PVDF was using a pre-amplifier designed in-house (gain: 23.5) while PZT was using a commercially available amplifier (gain: 25). PVDF has a much lower electromechanical coupling factor than PZT, which results in a

lower receive efficiency [38]. So, the signal PVDF received had a 30% smaller amplitude than that received by PZT (Fig. 6a and 6c).

The PVDF was also shown to capture a broad frequency range of signals generated by microbubbles (Fig. 6d and 7b). In contrast, the PZT could only receive signals at its odd-order resonant frequencies (Fig. 6b and 7a). Ultra-harmonics, even-order harmonics, and broadband signals captured with the PVDF were not observed in the signals captured with the PZT. Although there are designs using a second PZT transducer to receive microbubble emissions [13, 39, 40], the broadband frequency content of microbubbles is something that a PZT transducer could not fully accommodate. Furthermore, when broadband signals were generated, PZT's narrow bandwidth would distort the signal by showing a non-existing peak at its resonant frequency [1]. Current feedback control systems rely on the detection of harmonic and broadband signals, so it is important to avoid false positives. In the time domain, accurate signal waveforms can be used to identify potential harmful bubble behaviors, e.g., shock waves [41]. In the time domain, the PVDF (Fig. 6c) captured signals were shorter in duration, demonstrating a reduction in ringing artefacts. The high frequency data observed in the spectrum can also be clearly seen in the time domain data. Based on this data, the PVDF is better suited for detecting microbubble's acoustic emissions than PZT.

Our PZT and PVDF stacked transducer design was intended for a multi-element array, hence a simple structure was desired for mass production. By adding a layer of PVDF on the front, the design was simplified to a traditional piston transducer, where mainly the backing and matching layers of the PZT transmitter needed to be considered. As a result, it would be very easy to change the center frequency of the PZT; or transition to different materials, such as composite materials. The modular assembly process – where the PZT, PVDF, and two matching layers were assembled first, then backing and casing – avoided assembly errors and made the design more practical for mass production. Also, although we demonstrated a flat transducer design, it could be easily modified to a focused transducer. However, our intention is to use the flat transducer element as part of tens or hundreds of elements arranged on the surface of a hemispherical frame. The ultrasound generated by all the elements would be focused by this arrangement while allowing the ability to electronically steer the beam.

When incorporated into a multi-element array, our stacked transducers would have the transmission efficiency and reception efficiency for microbubble-seeded therapeutic applications. We selected Navy Type II PZT for our stacked transducer design, because we found it efficient enough for our short-duration and low-pressure therapeutic pulses [24, 27, 42]. For example, when using a rapid short pulse (RaSP) sequence to deliver drugs in the brain, we would need to produce a 5-cycle, 400-kPa pulse in the brain across the human skull. Without a matching network, our single element produced a peak-rarefactional pressure of 200 kPa at a 15-cm distance with a 300 V_{pp} input. The pressure at the geometric center of a multi-element hemispherical array can be roughly calculated as the sum of pressures generated by all elements. Assuming only 10-15% of the pressure can traverse the human skull to reach the sonication region at 1 MHz [43] , we estimate that an array of 20 stacked transducers could generate the 0.4 MPa required to deliver drugs across the BBB. As we can add more elements, add a matching network, and apply higher voltages [44], our transducer design should also be efficient enough to steer an ultrasound beam to different regions of the brain. On the receiving side, as ultrasound within 1- 2 MHz will attenuate after propagation through a human skull [45, 46], the signal-to-noise ratio (SNR) of the signal from one PVDF receiver (Fig. 6c) will be significantly reduced. Our rough calculation is that 10% signal transmission through the skull would lead to an approximate SNR reduction by 100 times. However, it may be possible to recover this loss in SNR by using hundreds to thousands of receiving elements [47] using passive acoustic mapping algorithms [48-50].

A limitation of our study was that the stacked transducer was not used to sonicate the microbubbles. Instead, a commercial transducer with the same center frequency as our PZT was used. However, we did not view this as a major shortcoming as the stacked transducer was designed to be incorporated into a multi-element array where the focal pressure will be the superposition of many stacked transducers. Furthermore, we have not yet evaluated how high the pressure generated by the PZT would affect the PVDF. A future improvement can be done by replacing the PZT with composite piezoelectric materials. As we needed to generate short pulses, we added a backing material that simultaneously reduced PZT's transmission efficiency. However, by using composite piezoelectric materials, we can avoid such a strong trade-off in transmission efficiency.

V. Conclusion

A PZT-PVDF stacked transducer for short-pulse ultrasound therapy and monitoring was presented. Taking merits of PVDF, the design was simplified to adding a PVDF receiver at the front surface of a traditional piston PZT transmitter. The stacked transducer showed its ability to transmit and receive short-pulse ultrasound from the same location. The PVDF was also shown to capture a broad frequency range of signals generated by microbubbles. These indicated its potential to compose a multi-element array for therapy and reliable monitoring. As the PVDF receiver didn't require backing or matching layers, this design could be easily adapted for different transmission frequencies or different transmitting materials. The simple structure and the adoption of a modular assembly process also made it practical for mass production. Future work will focus on incorporating this design into a multi-element transducer array.

REFERENCES

[1] N. McDannold, N. Vykhodtseva, and K. Hynynen, "Targeted disruption of the blood–brain barrier with focused ultrasound: association with cavitation activity," Physics in Medicine & Biology, vol. 51, p. 793, 2006.

[2] A. Sabraoui, C. Inserra, B. Gilles, J.-C. Béra, and J.-L. Mestas, "Feedback loop process to control acoustic cavitation," Ultrasonics sonochemistry, vol. 18, pp. 589-594, 2011.

[3] C.-W. Lo, C. Desjouy, S.-R. Chen, J.-L. Lee, C. Inserra, J.-C. Béra, et al., "Stabilizing in vitro ultrasound-mediated gene transfection by regulating cavitation," Ultrasonics sonochemistry, vol. 21, pp. 833-839, 2014.

[4] A. Razavi, D. Clement, R. A. Fowler, A. Birer, F. Chavrier, J.-l. Mestas, et al., "Contribution of inertial cavitation in the enhancement of in vitro transscleral drug delivery," Ultrasound in Medicine & Biology, vol. 40, pp. 1216-1227, 2014.

[5] K.-A. Saalbach, H. Ohrdes, and J. Twiefel, "Closed loop cavitation control–A step towards sonomechatronics," Ultrasonics sonochemistry, vol. 44, pp. 14-23, 2018.

[6] N. Lipsman, Y. Meng, A. J. Bethune, Y. Huang, B. Lam, M. Masellis, et al., "Blood–brain barrier opening in Alzheimer's disease using MR-guided focused ultrasound," Nature communications, vol. 9, p. 2336, 2018.

[7] M. A. O'Reilly and K. Hynynen, "Blood-brain barrier: Real-time feedback-controlled focused ultrasound disruption by using an acoustic emissions–based controller," Radiology, vol. 263, pp. 96-106, 2012.

[8] C. D. Arvanitis, M. S. Livingstone, N. Vykhodtseva, and N. McDannold, "Controlled ultrasound-induced blood-brain barrier disruption using passive acoustic emissions monitoring," PloS one, vol. 7, p. e45783, 2012.

[9] J. Ma, K. H. Martin, P. Li, P. A. Dayton, K. K. Shung, Q. Zhou, et al., "Design factors of intravascular dual frequency transducers for super-harmonic contrast imaging and acoustic angiography," Physics in Medicine & Biology, vol. 60, p. 3441, 2015.

[10] A. N. Pouliopoulos, S.-Y. Wu, M. T. Burgess, M. E. Karakatsani, H. A. Kamimura, and E. E. Konofagou, "A Clinical System for Non-invasive Blood–Brain Barrier Opening Using a Neuronavigation-Guided Single-Element Focused Ultrasound Transducer," Ultrasound in medicine & biology, 2019.

[11] J. Song and K. Hynynen, "Feasibility of using lateral mode coupling method for a large scale ultrasound phased array for noninvasive transcranial therapy," IEEE Transactions on Biomedical Engineering, vol. 57, pp. 124-133, 2010.

[12] Y. Huang, R. Alkins, M. L. Schwartz, and K. Hynynen, "Opening the blood-brain barrier with MR imaging–guided focused ultrasound: Preclinical testing on a trans–human skull porcine model," Radiology, vol. 282, pp. 123-130, 2016.

[13] S. V. Morse, T. Boltersdorf, B. I. Harriss, T. G. Chan, N. Baxan, H. S. Jung, et al., "Neuron labeling with rhodamine-conjugated Gd-based MRI contrast agents delivered to the brain via focused ultrasound," Theranostics, vol. 10, p. 2659, 2020.

[14] L. Deng, M. A. O'Reilly, R. M. Jones, R. An, and K. Hynynen, "A multi-frequency sparse hemispherical ultrasound phased array for microbubble-mediated transcranial therapy and simultaneous cavitation mapping," Physics in Medicine & Biology, vol. 61, pp. 8476-8501, 2011.

[15] M. A. O'Reilly and K. Hynynen, "A PVDF receiver for ultrasound monitoring of transcranial focused ultrasound therapy," IEEE transactions on Biomedical Engineering, vol. 57, pp. 2286-2294, 2010.

[16] T. Azuma, M. Ogihara, J. Kubota, A. Sasaki, S.-i. Umemura, and H. Furuhata, "Dual-frequency ultrasound imaging and therapeutic bilaminar array using frequency selective isolation layer," IEEE transactions on ultrasonics, ferroelectrics, and frequency control, vol. 57, pp. 1211-1224, 2010.

[17] P. Palanchon, A. Bouakaz, J. Klein, and N. de Jong, "Emboli detection using a new transducer design," Ultrasound in medicine & biology, vol. 30, pp. 123-126, 2004.

[18] I. Akiyama, S. Saito, and A. Ohya, "Development of an ultra-broadband ultrasonic imaging system: Prototype mechanical sector device," Journal of Medical Ultrasonics, vol. 33, pp. 71-76, 2006.

[19] L. Xiaozhou, Y. Shigong, G. Xiufen, Z. Weiya, and L. Rongrong, "Study of polymer ultrasonic transducer and complex ultrasonic transducer with PZT/PVDF multi-layer structure," Acta Acustica united with Acustica, vol. 85, pp. 420-426, 1999.

[20] K. Omote, K.-S. Park, G. Li, and H. Ohigashi, "Performance of multilayered ultrasonic transducers comprising vinylidene fluoride and trifluoroethylene copolymer films and ferroelectric ceramic plates," Japanese journal of applied physics, vol. 33, p. 2966, 1994.

[21] Z. Xu, M. Raghavan, T. L. Hall, C.-W. Chang, M.-A. Mycek, J. B. Fowlkes, et al., "High speed imaging of bubble clouds generated in pulsed ultrasound cavitational therapy-histotripsy," IEEE transactions on ultrasonics, ferroelectrics, and frequency control, vol. 54, pp. 2091-2101, 2007.

[22] Z. Xu, T. L. Hall, J. B. Fowlkes, and C. A. Cain, "Effects of acoustic parameters on bubble cloud dynamics in ultrasound tissue erosion (histotripsy)," The Journal of the Acoustical Society of America, vol. 122, pp. 229-236, 2007.

[23] J. J. Choi, K. Selert, Z. Gao, G. Samiotaki, B. Baseri, and E. E. Konofagou, "Noninvasive and localized blood—brain barrier disruption using focused ultrasound can be achieved at short pulse lengths and low pulse repetition frequencies," Journal of Cerebral Blood Flow & Metabolism, vol. 31, pp. 725-737, 2011.

[24] J. J. Choi, K. Selert, F. Vlachos, A. Wong, and E. E. Konofagou, "Noninvasive and localized neuronal delivery using short ultrasonic pulses and microbubbles," Proceedings of the National Academy of Sciences, vol. 108, pp. 16539-16544, 2011.

[25] M. A. O'Reilly, A. C. Waspe, M. Ganguly, and K. Hynynen, "Focused-ultrasound disruption of the blood-brain barrier using closely-timed short pulses: influence of sonication parameters and injection rate," Ultrasound in medicine & biology, vol. 37, pp. 587-594, 2011.

[26] M. A. O'Reilly, Y. Huang, and K. Hynynen, "The impact of standing wave effects on transcranial focused ultrasound disruption of the blood–brain barrier in a rat model," Physics in Medicine & Biology, vol. 55, p. 5251, 2010.

[27] S. V. Morse, A. N. Pouliopoulos, T. G. Chan, M. J. Copping, J. Lin, N. J. Long, et al., "Rapid Short-pulse Ultrasound Delivers Drugs Uniformly across the Murine Blood-Brain Barrier with Negligible Disruption," Radiology, p. 181625, 2019.

[28] K. K. Shung, J. Cannata, and Q. Zhou, "Piezoelectric materials for high frequency medical imaging applications: A review," Journal of Electroceramics, vol. 19, pp. 141-147, 2007.

[29] A. D. Maxwell, "Noninvasive Thrombolysis Using Histotripsy Pulsed Ultrasound Cavitation Therapy," 2012.

[30] C. S. Desilets, J. D. Fraser, and G. S. Kino, "The design of efficient broad-band piezoelectric transducers," IEEE Transactions on sonics and ultrasonics, vol. 25, pp. 115-125, 1978.

[31] J. R. Tse and A. J. Engler, "Preparation of hydrogel substrates with tunable mechanical properties," Current protocols in cell biology, vol. 47, pp. 10.16. 1-10.16. 16, 2010.

[32] A. N. Pouliopoulos, "Controlling microbubble dynamics in ultrasound therapy," 2016.

[33] A. N. Pouliopoulos, S. Bonaccorsi, and J. J. Choi, "Exploiting flow to control the in vitro spatiotemporal distribution of microbubble-seeded acoustic cavitation activity in ultrasound therapy," Physics in Medicine & Biology, vol. 59, p. 6941, 2014.

[34] T. Leighton, P. White, C. Morfey, J. Clarke, G. Heald, H. Dumbrell, et al., "The effect of reverberation on the damping of bubbles," The Journal of the Acoustical Society of America, vol. 112, pp. 1366-1376, 2002.

[35] J. M. Cannata, T. A. Ritter, W.-H. Chen, R. H. Silverman, and K. K. Shung, "Design of efficient, broadband single-element (20-80 MHz) ultrasonic transducers for medical imaging applications," IEEE transactions on ultrasonics, ferroelectrics, and frequency control, vol. 50, pp. 1548-1557, 2003.

[36] H. Fang, Y. Chen, C. Wong, W. Qiu, H. Chan, J. Dai, et al., "Anodic aluminum oxide–epoxy composite acoustic matching layers for ultrasonic transducer application," Ultrasonics, vol. 70, pp. 29-33, 2016.

[37] Q. Zhou, K. H. Lam, H. Zheng, W. Qiu, and K. K. Shung, "Piezoelectric single crystal ultrasonic transducers for biomedical applications," Progress in materials science, vol. 66, pp. 87-111, 2014.

[38] K. Nakamura, Ultrasonic transducers: Materials and design for sensors, actuators and medical applications: Elsevier, 2012.

[39] C. D. Arvanitis, M. Bazan-Peregrino, B. Rifai, L. W. Seymour, and C. C. Coussios, "Cavitation-enhanced extravasation for drug delivery," Ultrasound in medicine & biology, vol. 37, pp. 1838-1852, 2011.

[40] C. Jensen, R. Cleveland, and C. Coussios, "Real-time temperature estimation and monitoring of HIFU ablation through a combined modeling and passive acoustic mapping approach," Physics in Medicine & Biology, vol. 58, p. 5833, 2013.

[41] K. Johansen, J. H. Song, and P. Prentice, "Performance characterisation of a passive cavitation detector optimised for subharmonic periodic shock

waves from acoustic cavitation in MHz and sub-MHz ultrasound," Ultrasonics sonochemistry, vol. 43, pp. 146-155, 2018.

[42] M. A. O'Reilly, Y. Huang, and K. Hynynen, "The impact of standing wave effects on transcranial focused ultrasound disruption of the blood-brain barrier in a rat model," Physics in Medicine & Biology, vol. 55, pp. 5251-67, 2010.

[43] D. Pajek and K. Hynynen, "The design of a focused ultrasound transducer array for the treatment of stroke: a simulation study," Physics in Medicine & Biology, vol. 57, p. 4951, 2012.

[44] Y. Li, T. L. Hall, Z. Xu, and C. A. Cain, "Enhanced shock scattering histotripsy with pseudo-monopolar ultrasound pulses," IEEE transactions on ultrasonics, ferroelectrics, and frequency control, 2019.

[45] A. Y. Ammi, T. D. Mast, I.-H. Huang, T. A. Abruzzo, C.-C. Coussios, G. J. Shaw, et al., "Characterization of ultrasound propagation through ex-vivo human temporal bone," Ultrasound in medicine & biology, vol. 34, pp. 1578-1589, 2008.

[46] L. Deng, M. A. O'Reilly, R. M. Jones, R. An, and K. Hynynen, "A multi-frequency sparse hemispherical ultrasound phased array for microbubble-mediated transcranial therapy and simultaneous cavitation mapping," Physics in Medicine & Biology, vol. 61, p. 8476, 2016.

[47] R. M. Jones, M. A. O'Reilly, and K. Hynynen, "Transcranial passive acoustic mapping with hemispherical sparse arrays using CT-based skull-specific aberration corrections: a simulation study," Physics in Medicine & Biology, vol. 58, p. 4981, 2013.

[48] M. Gyöngy and C.-C. Coussios, "Passive cavitation mapping for localization and tracking of bubble dynamics," The Journal of the Acoustical Society of America, vol. 128, pp. EL175-EL180, 2010.

[49] H. J. Davies, S. V. Morse, M. J. Copping, K. Sujarittam, V. D. Bourgin, M.-X. Tang, et al., "Imaging with Therapeutic Acoustic Wavelets–Short Pulses Enable Acoustic Localisation when Time of Arrival is Combined with Delay and Sum," IEEE Transactions on Ultrasonics, Ferroelectrics, and Frequency Control, 2020.

[50] J. J. Choi, R. C. Carlisle, C. Coviello, L. Seymour, and C.-C. Coussios, "Non-invasive and real-time passive acoustic mapping of ultrasound-mediated drug delivery," Physics in Medicine & Biology, vol. 59, p. 4861, 2014.

Zheng Jiang was born in Jiangsu, China, in 1993. He was awarded an M.Eng degree in Mechanical Engineering and Theory from State Key Laboratory of Mechanics and Control of Mechanical Structures, Nanjing University of Aeronautics and Astronautics, Nanjing, China in 2018, and a B.Eng degree in Aircraft Airworthiness Technology (Aircraft Design and Engineering) from Nanjing University of Aeronautics and Astronautics, Nanjing, China in 2015. He is currently a Ph.D. student with the Department of Bioengineering, Imperial College London. His research interests include ultrasound transducer design, ultrasound field simulation, and skull imaging.

Robert J. Dickinson graduated with a degree in physics from Cambridge University, England, and then obtained a PhD in Biophysics from the University of London, in ultrasound signal processing.

He is a Senior Lecturer at the Department of Bio-engineering, Imperial College London. He worked on MRI coil development and system integration at Picker International Ltd and ultrasound imaging in a start-up company Intravascular Research Ltd where he developed a sub-1mm intravascular ultrasound imaging catheter. He has substantial experience in the bio-compatibility, electrical safety and other issues of invasive medical devices, together with commercialization and IP transfer. He has 14 granted patents and over 60 published papers, and has commercialized 8 medical devices. He has recently worked with Emcision Ltd on their range of electrosurgical devices and both LimFlow SA and Pathfinder Medical Ltd on percutaneous anastomosis devices.

Dr. Dickinson is Chartered Engineer, a member of the Institute of Physics and Institute of Physics and Engineering in Medicine.

Timothy L. Hall was born in Lansing, MI, USA, in 1975. He received the B.S.E. and M.S.E. degrees in electrical engineering and the Ph.D. degree in biomedical engineering from the University of Michigan, Ann Arbor, MI, USA, in 1998, 2001, and 2007, respectively. He worked for Teradyne Inc., Boston, MA, USA, from 1998 to 1999, as a circuit design engineer and at the University of Michigan, from 2001 to 2004, as a visiting research investigator. He is currently an Associate Research Scientist in the Department of Biomedical Engineering at the University of Michigan. His research interests are in high-power pulsed RF-amplifier electronics, phased-array ultrasound transducers for therapeutics, and sonic cavitation for therapeutic applications.

James J. Choi is a Senior Lecturer at the Department of Bioengineering at Imperial College London and leads the Noninvasive Surgery & Biopsy Laboratory. He received the B.S.E. degree in computer engineering at the University of Michigan, Ann Arbor, MI, USA, while studying pre-medicine. He obtained the Ph.D. degree in Biomedical Engineering at Columbia University, New York, NY, USA, where he developed ultrasound technologies that noninvasively and locally alter blood-brain barrier permeability. He then conducted postdoctoral research at the University of Oxford, Oxford, United Kingdom, where he developed passive acoustic mapping methods and ultrasound drug delivery and release technologies. He was awarded the Frederick V. Hunt Postdoctoral Research Fellowship in Acoustics in 2011- 2012. In 2013, he founded the Noninvasive Surgery & Biopsy Laboratory at Imperial College London, London, United Kingdom, whose mission is to create the next generation of noninvasive microsurgical devices for the treatment and diagnosis of diseases.